A major purpose of the Technical Information Center is to provide the broadest dissemination possible of information contained in DOE's Research and Development Reports to business, industry, the academic community, and federal, state and local governments.

Although portions of this report are not reproducible, it is being made available in microfiche to facilitate the availability of those parts of the document which are legible.

3

LA-UR -84-1621

NOTICE

THIS REPORT IS ILLEGIBLE TO A DEGREE
THAT PRECLUDES SATISFACTORY REPRODUCTION

DR-1448-6

Los Alamos National Laboratory is operated by the University of California for the United States Department of Energy under contract W-7405-ENG-36

CONF-8308172--1

TITLE: High-Strain-Rate Measurements of Dislocation Mobility

LA-UR--84-1621

DE84 012448

AUTHOR(S): P. S. Follansbee, G. Regazzoni, U. F. Kocks

SUBMITTED TO: Proceedings of International Symposium on Mechanics of Dislocations, Houghton, Michigan August 28-31, 1983

DISCLAIMER

This report was prepared as an account of work sponsored by an agency of the United States Government. Neither the United States Government nor any agency thereof, nor any of their employees, makes any warranty, express or implied, or assumes any legal liability or responsibility for the accuracy, completeness, or usefulness of any information, apparatus, product, or process disclosed, or represents that its use would not infringe privately owned rights. Reference herein to any specific commercial product, process, or service by trade name, trademark, manufacturer, or otherwise does not necessarily constitute or imply its endorsement, recommendation, or favoring by the United States Government or any agency thereof. The views and opinions of authors expressed herein do not necessarily state or reflect those of the United States Government or any agency thereof.

MASTER

By acceptance of this article, the publisher recognizes that the U.S. Government retains a nonexclusive, royalty-free license to publish or reproduce the published form of this contribution, or to allow others to do so, for U.S. Government purposes.

The Los Alamos National Laboratory requests that the publisher identify this article as work performed under the auspices of the U.S. Department of Energy

Los Alamos National Laboratory
Los Alamos, New Mexico 87545

FORM NO. 836 R4

High-Strain-Rate Measurements of Dislocation Mobility

P. S. Follansbee, G. Regazzoni and U. F. Kocks

Materials Science and Technology Division
Los Alamos National Laboratory
Los Alamos, NM 87545 USA

ABSTRACT

The strain rate sensitivity in a variety of metals is known to increase dramatically when the strain rate exceeds about 10^3 s^{-1}. In copper, this behavior is analyzed in terms of the transition in rate controlling deformation mechanism from thermal activation to dislocation drag. Experimental results can be made to agree with a model of this transition, which leads to several observations regarding dislocation mobility at these high strain rates. The mobile dislocation density is estimated to be a mildly increasing function of stress or strain rate at any one strain and is roughly independent of strain for $0.05 < \varepsilon < 0.20$.

1. INTRODUCTION

The mobile dislocation density assumes an important role in deformation processes, but determination of its value has not been possible with direct experimental procedures. Although it is now claimed that such a measurement is possible using nuclear magnetic resonance techniques (Tamler et al, 1981), determination of the mobile dislocation density previously has relied on indirect measurements such as the analysis of stress relaxation data (for a review, see Aifantis and Gerberich, 1975), quantitative investigation of the Portevin-Le Chatelier effect (Mayer et al, 1980), and direct observations in the transmission electron microscope of dislocation generation and motion during in situ deformation (Orlova, 1981).

The results of measurements at high strain rates also have been interpreted in terms of dislocation mobility. This has resulted from the observed increase in rate sensitivity in a variety of metals when the strain rate exceeds about 10^3 s^{-1}. (See, for example, Hauser et al,

1961, for experimental results on aluminum and Kumar and Kumble, 1969, for results on copper.) The change in rate sensitivity has been interpeted as a transition in rate controlling deformation mechanism with increasing strain rate, and the increased strain rate sensitivity has been thought to indicate the emergence of dislocation drag as the rate controlling deformation mechanism. That is, when the applied stress σ is raised above some critical level, thermal activation is no longer necessary to assist a dislocation past a barrier and dislocation motion becomes limited only by dissipative forces during continuous glide. The continuous motion of a dislocation moving through a lattice is resisted by the lattice potential itself, as well as by interactions with phonons, electrons, radiation and point defects. These dissipative processes, which have been described in detail by Granato (1973), are viscous in nature and lead to a linear dependence of the dislocation velocity V on the net driving force $\sigma_e b$ according to

$$V = \sigma_e b / MB \qquad (1)$$

where B is the drag coefficient, σ_e is some effective stress on the dislocation (yet to be more closely defined), M is the average Taylor factor, and b is the Burgers vector. In copper at room temperature phonon drag is thought to provide the dominant resistance to dislocation motion. The drag coefficient is available from independent measurements; a value of $B = 4.3 \times 10^{-5}$ Pa s represents an average of values reported in the literature for copper at room temperature (see, for example, Vreeland, 1968).

If the average dislocation velocity is known from Eq. (1) then the mobile dislocation density can be deduced from the kinematic relation between strain rate $\dot{\epsilon}$, mobile dislocation density ρ_m, and average dislocation velocity,

$$\dot{\epsilon} = \rho_m bv/M \ . \tag{2}$$

Equations (1) and (2) combine to yield

$$\dot{\epsilon} = \frac{b^2\rho_m}{M^2 B}\sigma_e \ . \tag{3}$$

Previous investigators have taken σ_e as the overstress (Kumar et al, 1968),

$$\sigma_e = \sigma - \hat{\tau} \ , \tag{4}$$

where $\hat{\tau}$ is a threshold stress. Substituting Eq. (4) into (3) gives

$$\sigma = \sigma_b + \beta\dot{\epsilon} \ , \tag{5}$$

where

$$\sigma_b = \hat{\tau} \ , \text{ and} \tag{6}$$

$$\beta = \frac{M^2 B}{b^2\rho_m} \ . \tag{7}$$

When the mobile dislocation density is constant, Eq. (5) indicates that the flow stress should vary linearly with strain rate. This is indeed what is usually observed in high strain rate measurements on copper and aluminum, which has led to estimates of ρ_m from Eq. (7). There also has been evidence (Kumar et al, 1968) that σ_b and its variation with strain were consistent with the expected behavior of the back stress.

There have been, however, serious objections to Eq. (4) on theoretical grounds; these will be reviewed in the next section. Extensive experimental results on copper deformed at high strain rates are presented in section 3 and the dynamic flow stress is compared with the value of the threshold stress measured independently. A dislocation model of the deformation kinetics is used in section 4 and can be made to agree quite well with the data. In section 5 the mobile dislocation density consistent with the model is discussed; it is approximately constant with strain, but increases with a small power of stress at constant structure. These results are discussed in light of the current understanding of microstructural deformation mechanisms in copper.

2. THE KINETICS OF GLIDE

The inconsistency in the interpretation presented above lies in the assumption described by Eq. (4). In order to see this it is necessary to review deformation mechanisms in copper at low strains. In this material, deformation proceeds by the motion of dislocations. Seeger (1955) suggested that at room temperature the intersection of glissile dislocations with sessile forest dislocations restricts deformation and that the overcoming of such an obstacle is a thermally activated process. It is well known that dislocations rapidly multiply with increased strain, and that most of the dislocations eventually become tied up in intense tangles which can form cell-like structures. According to one model (Kocks,

1975), the walls of tangled dislocations make up hard regions that can not be penetrated by the mobile dislocations and that separate the soft inner regions. Continued deformation proceeds by the motion of dislocations through these soft regions. A schematic of such a tangled structure, as proposed by Shioiri et al (1978), is shown in Fig. 1. It is proposed that the application of stress, assisted by thermal activation, forces the expansion of loops from the tangles, as shown in Fig. 1. These loops will move through the soft regions until their motion becomes impeded by another tangle.

The dislocation interactions in an ensemble such as that shown in Fig. 1 are complicated and highly statistical. However, the resistance felt by a single, average dislocation as it moves along its glide plane can be summarized by the resistance profile shown in Fig. 2 which is taken from Kocks, Argon, and Ashby (1975). The two large excursions in this figure represent barriers of width λ_1 separated by a distance λ_2. The height of the barrier is the threshold stress which is the flow stress at T = 0 K. Between the barriers the glide resistance is small; it is on the average non-zero by no more than the rate of energy storage with plastic strain. For simplicity it is assumed during the remaining discussion that the glide resistance is zero in this region. As has been discussed, thermal activation is rate controlling when the applied stress (σ_1) is less than the threshold stress, whereas at a stress (σ_2) greater than this critical value dislocations are no longer held up at barriers and the dislocation velocity is determined solely by drag phenomena. At any position y along the glide plane the driving force on the dislocation is (apart from a resolving factor)*

$$\sigma_e(y)\, b = [\sigma - \tau(y)]\, b \,. \qquad (8)$$

It is clear from Eq. (8) and Fig. 2 that Eq. (4) only applies when the dislocation is directly over an obstacle; the majority of time during continuous glide the driving force is simply σb. The actual dislocation velocity is determined by averaging times spent at all positions along the glide plane. When λ_2 is much greater than λ_1 the average effective stress reduces to the applied stress.

The average dislocation velocity is expected to follow that shown schematically in Fig. 3 (Clifton, 1971, Kocks et al, 1975). At applied stresses below the threshold stress the velocity is low as a dislocation spends most of the time awaiting thermal activation. At stresses above the threshold stress the dislocation velocity approaches the drag controlled limit. The dashed curves in Fig. 3 show that the rate at which this limit is approached depends on the ratio λ_2/λ_1. The

*Both the threshold stress $\hat{\tau}$ and the applied stress σ are used here as tensile stresses.

spacing between barriers in the model shown in Fig. 1 is expected to be on the order of microns, whereas the width of the obstacle is expected to be on the order of a few Burgers vectors. Thus λ_2/λ_1 is expected to be a large number and, when the applied stress exceeds the threshold stress, the drag controlled limit should be approached rapidly.

Relativistic effects restrict the dislocation velocity to the speed of sound C_s and, as is shown in Fig. 3, this limit should be approached asymptotically. Although there is no absolute rule as to when these effects must be considered, Weertman (1973) has suggested that deviations from Eq. (1) may begin at one-third of the shear wave velocity, which from Eq. (1) corresponds to a stress of ~400 MPa for copper.

Another mechanism that is expected to affect the interaction between a moving dislocation and an obstacle is inertia. Inertial effects can influence the transition in two ways: first, they prevent the dislocation from instantaneously reaching its drag-controlled velocity when a stress is suddenly applied. This effect is probably negligible for the model considered here since the characteristic time for the dislocation to reach its limiting velocity is approximately 10^{-11} s (Kocks et al, 1975) which is several orders of magnitude less than the time spent running between two obstacles. Inertia also can prevent a dislocation from instantaneously stopping when the driving force suddenly drops to zero. This effect can assist the dislocation in overcoming an obstacle, and its influence can be easily evaluated through the dimensionless ratio (Kocks et al, 1975)

$$\frac{y_{stop}}{b} = \frac{\sigma\rho b^2}{2MB^2}, \qquad (9)$$

where ρ is the density of the material and y_{stop} is the stopping distance of a dislocation moving at its drag controlled velocity under a stress of σ. For the case of copper the ratio is computed to be ~4. This value is an upper limit since it considers an instantaneous change in the driving force. As shown in Fig. 2, the driving force decreases to zero over a distance $\lambda_1/2$ which, as has been noted, is on the order of a few Burger's vectors; thus, it is not expected that inertia influences the transition regime in copper deformed at room temperature. At low temperature, where the value of the drag coefficient decreases significantly, it is well known that obstacles can be overcome inertially (Granato, 1971).

When the mobile dislocation density is constant the ordinate of Fig. 3 is directly proportional to the strain rate from Eq. (3). This implies that if the experimental results referred to earlier are truly in the drag controlled regime then the linear plot of strain

rate versus stress should extrapolate through the origin. This is in contrast to the observed behavior in which σ_h in Eq. (3) is a large fraction of σ itself. Klahn et al (1970) and Frost and Ashby (1971) noted this discrepancy between the experimental results and predicted behavior. In the latter reference it was suggested that a mobile dislocation density that increased with strain rate could provide the link between the observations and theory. This motivated the series of experiments on copper that are described in the next section. In particular, a measurement of the threshold stress on dynamically deformed material is reported which enables a comparison of the test results with the behavior predicted from the dependence of dislocation velocity with applied stress shown in Fig. 3.

3. EXPERIMENTAL PROCEDURES AND RESULTS

High conductivity electrolytic copper (ASTM C10100) was chosen as a test material. Cylindrical samples for compression tests were machined and annealed at 600 C for one hour to yield the desired recrystallized grain structure with equiaxed grains of approximately 37 μm in average dimension. Low-strain-rate tests were performed with specimens 5.1 mm in both diameter and length in a standard screw-driven mechanical test machine with a subpress to insure parallel surfaces. Tests at strain rates of 1 s^{-1} and 30 s^{-1} were performed, also using a subpress, in a hydraulic testing machine. High-strain-rate tests were performed in a split Hopkinson pressure bar (SHPB) using an experimental technique similar to that described by Lindholm (1971). Three pairs of pressure bars (9.3 mm, 6.3 mm, and 4.7 mm diameter) were employed to cover the strain range of 10^3 s^{-1} to $3x10^4$ s^{-1}. The experimental procedures have been described in more detail by Follansbee, Regazzoni, and Kocks (1984) and by Frantz, Follansbee, and Wright (1984).

Stress strain curves at strain rates of $2x10^{-3}$ s^{-1}, 1 s^{-1}, $6x10^3$ s^{-1} and $2.4x10^4$ s^{-1} are shown in Fig. 4. The oscillations in the two curves at the highest strain rates are due to elastic wave dispersion in the pressure bars; a numerical correction procedure (Follansbee and Frantz, 1983) has been applied to minimize these effects. Data at low strains in the two high strain rate curves is not included in this figure since initially the specimen does not deform uniformly.

The stress strain curves in Fig. 4 indicate that the strain rate sensitivity increases when the strain rate is raised above ~10^3 s^{-1}. This is even more evident in Fig. 5, which is a plot of flow stress at a constant true strain of 0.15 versus the logarithm of strain rate for all of the measurements. The results at strains of 0.05, 0.10, and 0.20 are qualitatively identical to those shown in Fig. 5. Typical of previous

experimental results, the strain rate sensitivity is relatively mild at low strain rates but increases dramatically when the strain rate is raised above approximately 10^3 s^{-1}.

A plot of the high strain rate data on a linear strain rate axis is shown in Fig. 6. (The significance of the dashed line in this figure is described in the following section.) Note in this figure that different symbols are used to represent results from pressure bars of different diameter. The general agreement between the results from these bars provides confidence in the measurements. As found previously, the data closely follow Eq. (2). The values of σ_b and B for strains of 0.05 to 0.20 are listed below.

ε	σ_b, MPa	B, MPa s
0.05	114	0.00353
0.10	188	0.00356
0.15	248	0.00312
0.20	290	0.00263

3.1 MEASUREMENT OF THE THRESHOLD STRESS - The interpretation of the experimental results shown in Fig. 5 in terms of the continuous glide model requires a comparison of the dynamic flow stress with the threshold stress, the value of which was estimated in the following manner. Ten specimens were deformed identically at a strain rate of 5.5×10^3 s^{-1} to a true strain of 0.144. The specimens were stored at liquid N_2 temperature until each could be reloaded statically at various temperatures as indicated in Fig. 7. The stress at which plastic flow resumed was recorded at each temperature. The threshold stress is the flow stress at 0 K, which requires an extrapolation of the experimental results. Consistent with an appropriate thermal activation law for jerky glide (Kocks et al, 1975),

$$\dot{\varepsilon} = \dot{\varepsilon}_o \exp\left\{ -F_o/kT \left[1-\left(\sigma/\hat{\tau}\right)^{1/2}\right]^{3/2} \right\} , \qquad (10)$$

the data were plotted as $\sigma^{1/2}$ versus $T^{2/3}$ and a linear extrapolation was made as illustrated in Fig. 8; the threshold stress is approximately 350 MPa at a true strain of 0.144. A small correction is required to refer the threshold stress to a true strain of 0.15. The threshold stress should vary with the square root of the total dislocation density which increases roughly linearly with plastic strain (Edington, 1969). This trivial correction yields a threshold stress of 355 MPa at a true strain of 0.15.

This value of the threshold stress is included in Fig. 6 as a dashed line. Although the measurement of the threshold stress strictly applies to the structure produced at a strain rate of 5.5×10^3 s^{-1}, it is assumed here that a comparison at constant strain approximates a

comparison at constant structure. That is, it is assumed in the remaining discussion that the threshold stress is independent of strain rate. This is an important assumption which is discussed in more detail later.

The comparison of the experimental results in Fig. 6 with the predicted behavior as described in Fig. 3 leads to two observations. The first is that all of the experimental results lie below the measured threshold stress. The second observation is that the apparent transition occurs at a stress that is 75% to 80% of the threshold stress. Explanations for these findings will be explored with a model of the deformation kinetics which is described in the next section.

4. DEFORMATION KINETICS IN THE TRANSITION REGIME

Previous investigators have modelled with various degrees of complexity the transition from thermally activated to dislocation drag controlled deformation by summing the times spent awaiting thermal activation energy to overcome a barrier and that spent moving to the next barrier. Models that consider an ensemble of barriers and actual dislocation configurations between these barriers have been proposed by Frost and Ashby (1971) and Klahn et al (1970) while simpler models that consider only the interaction of a single straight dislocation with a barrier have been described by Kumar and Kumble (1969), Clifton (1971) and Shioiri et al (1978). The latter approach is adopted here to compare with the experimental results presented above.

Following these previous investigators, the dislocation velocity is

$$V = \frac{\lambda_2}{t_w + t_r} \tag{11}$$

where t_w is the waiting time given by the thermal activation equation

$$t_w = \nu_o^{-1} \exp \Delta G/kT \tag{12}$$

and $$\Delta G = F_o\left[1-\left(\sigma/\hat{\tau}\right)^{1/2}\right]^{3/2} . \tag{13}$$

The running time t_r is given by

$$t_r = MB\lambda_2/\sigma b . \tag{14}$$

Combining Eqs. (3) and (11) through (14) gives

$$\dot{\varepsilon} = \frac{\hat{\dot{\varepsilon}}\ \sigma/\hat{\tau}}{1 + \Psi\ \sigma/\hat{\tau}\ \exp \Delta G/kT} \tag{15}$$

where $$\hat{\dot{\varepsilon}} = \frac{b^2 \rho_m \hat{\tau}}{M^2 B}, \tag{16}$$

and is the strain rate at which the transition is complete,

and $$\Psi = \frac{\nu_o^{-1} b\hat{\tau}}{MB\lambda_2} . \tag{17}$$

The variables in Eqs. (15) through (17) are λ_2, ρ_m and F_0. The attempt frequency ν_0 may be taken as 10^{11} s^{-1}, the average Taylor factor is 3.1, and a value of β has been quoted previously ($\beta = 4.3\times10^{-5}$ Pa s). The dimensionless quantity F_0/kT can be related to the constant-structure strain rate sensitivity parameter m, where

$$m = \frac{\partial \ln \dot{\epsilon}}{\partial \ln \sigma}\Big|_T \quad . \tag{18}$$

The slope of the low strain rate results in Fig. 5 yields a m-value of 70 which corresponds to $F_0/kT = 220$. This is a higher strain rate sensitivity than is typical for dislocation - obstacle interactions in pure fcc metals (Mecking and Kocks, 1980). One mechanism that could be responsible for m = 70 is dynamic recovery. When dynamic recovery is important, the threshold stress at a uniform strain should vary with strain rate. Then the constant structure model used here should not be strictly applicable to the constant strain experimental comparison shown in Figs. 5 and 6. We have neglected this effect in this paper and will proceed under this assumption.

Predictions of the model for various values of λ_2 and ρ_m are illustrated in Fig. 9 which is a plot of $\sigma/\hat{\tau}$ versus ϵ. It is evident in Fig. 9 that, within the transition regime, the model is more sensitive to the value of ρ_m than it is to λ_2. Furthermore, Fig. 9 shows that ρ_m and λ_2 are not independent; if ρ_m is chosen to match results in the transition regime, then the value of λ_2 is constrained by the low strain rate results.

A constant mobile dislocation density of 5.7×10^{11} m^{-2} yields the predicted curve shown in Fig. 10 which also includes the experimental data points at a strain of 0.15 and the measured value of $\hat{\tau}$. The deduced value of λ_2 is 40 μm. (We consider this estimate of λ_2 to be too large; this also could be a result of the uncharacteristic m-value at low strain rates.) The comparison in Fig. 10 verifies that the transition begins at a stress below the threshold stress, as found experimentally. However, the model clearly indicates an inflection point in the vicinity of $\hat{\tau}$, whereas the experimental results continue to follow the trend of Eq. (2). This divergence between the predictions of the model and the experimental results could be due to the assumption regarding the mobile dislocation density and will be discussed in the following section.

5. THE MOBILE DISLOCATION DENSITY

5.1 THE STRAIN DEPENDENCE OF ρ_m - In the model developed in the previous section it has been explicitly assumed that the mobile dislocation density is independent of strain rate (or stress) at constant structure. Perhaps an explanation for the lack of an inflection

near the threshold stress is that, as proposed by Frost and Ashby (1971), the mobile dislocation density is an increasing function of stress. One way to introduce a stress dependence of the mobile dislocation density is to write

$$\rho_m = \rho_m^o (\sigma/\hat{\tau})^n . \tag{19}$$

The predictions of the model for $n = 2$ (solid line) and $n = 3$ (dashed line) are shown in Fig. 11 along with the experimental results. For these comparisons the value of ρ_m^o is taken as the constant value of ρ_m found previously (3.7×10^{11} m^{-2}). The agreement improves in the transition regime over that shown in Fig. 10. The solid line in Fig. 5 demonstrates the comparison with $n = 2$ over the entire strain rate range.

In these measurements, there are insufficient data at stresses above the threshold stress to further evaluate the stress dependence of the mobile dislocation density. However, Clifton, Gilat and Li (1983) have made measurements at higher strain rates using the pressure-shear experiment on similar material. A data point at a uniaxial strain of 0.05 (the highest strain reached in this experiment) is combined with the Hopkinson bar measurements at the same strain in Fig. 12. Included in this figure is the prediction of the model for $n = 2$, which gives good agreement with the higher strain rate data point. (The determination of $\hat{\tau}$ at a strain of 0.05 is described below.) It is thus concluded that an increasing mobile dislocation density could explain the deviation between the observed and predicted behavior near and above $\hat{\tau}$.

5.2 THE STRAIN DEPENDENCE OF ρ_m - The results presented in Figs. 10 and 11 referred to only one strain ($\varepsilon = 0.15$). To investigate the strain dependence of ρ_m the following normalization scheme is used. Introducing Eq. (19) for the stress dependence of the mobile dislocation density into Eq. (15) and rearranging yields

$$\frac{\dot{\varepsilon}}{\dot{\varepsilon}_o} = \frac{(\sigma/\hat{\tau})^{n+1}}{1 + \bar{\tau}\, \sigma/\hat{\tau} \exp \Delta G/kT} , \tag{20}$$

where

$$\dot{\varepsilon}_o = \frac{b^2 \rho_m^o \hat{\tau}}{M^2 B} . \tag{21}$$

Inspection of Eq. (20) suggests that a plot of $\dot{\varepsilon}/\dot{\varepsilon}_o$ versus $\sigma/\hat{\tau}$ varies with strain only to the extent that $\bar{\tau}$ does (assuming that F_o/kT is independent of strain, which is true for this material). However, when $\bar{\tau}$ is small with respect to one, the plot should be approximately invariant with strain. Thus, by choosing $\dot{\varepsilon}_o(\varepsilon)$ and $\hat{\tau}(\varepsilon)$ to give the best correlation of all the experimental results, the $\rho_m(\varepsilon)$ dependence can be extracted directly from Eq. (21). Figure 13

shows the fit obtained at strains of 0.05, 0.12, 0.15, and 0.20 and the theoretical prediction (solid line) for $n = 2$ and $\rho_m^o = 5.7\times10^{11}\ m^{-2}$ in Eq. (19). (A dashed line is drawn at the drag controlled limit.) The fitting parameters and the deduced mobile dislocation density are listed in the following table.

ϵ	$\hat{\tau}$	$\hat{\dot{\epsilon}}_o$	$\rho_m(\dot{\epsilon} = 1.5\times10^4\ s^{-1})$
	MPa	$10^4\ s^{-1}$	$10^{11}\ m^{-2}$
0.05	170	1.6	5.1
0.10	275	2.5	4.6
0.15	355	3.3	4.1
0.20	415	3.9	3.7

The $\hat{\tau}(\epsilon)$ dependence is seen to be slightly stronger than the square-root dependence estimated in section 3.1. It also is evident that ρ_m remains approximately constant, or even decreases slightly, over the strain range investigated. (The small decrease noted in ρ_m may not be outside the uncertainty in the above normalization procedure.) This result is in contrast to that expected for the total dislocation density which increases by a factor of four within the same strain range (Edington, 1969). Thus, the ratio of the mobile to the total dislocation density decreases with increasing strain. In fact, from Edington's measurements of the total dislocation density and its variation with strain, the ratio decreases from $\sim1\times10^{-2}$ to $\sim2\times10^{-3}$ when the strain increases from 0.05 to 0.20 at a strain rate of $1.5\times10^4\ s^{-1}$.

5.3 DISCUSSION - The observations regarding the stress and strain dependence of the mobile dislocation density noted above are compatible with each other and with the microstructural model of deformation in copper proposed in section 2. We note that since both σ and τ are found to increase roughly with the square-root of strain, their ratio remains approximately constant,

$$\left.\frac{\sigma}{\hat{\tau}}\right]_{\epsilon} = \text{constant}. \qquad (22)$$

(As shown above, $\hat{\tau}$ increases slightly more rapidly; thus, the ratio σ/τ actually decreases slightly with increasing strain.) Equation 22 is typical for thermally activated controlled deformation (Mecking and Kocks, 1981). However, it is not obvious why Eq. (22) should persist as dislocation drag becomes rate controlling.

Under the assumption that $\sigma/\hat{\tau}$ remains constant, the strain dependence of ρ_m is easily seen by simplifying Eq. (15) to read

$$\dot{\epsilon} = \rho_m(\epsilon)\ \hat{\tau}(\epsilon)\ f(\hat{\tau})\ , \qquad (23)$$

where the function f varies with $\hat{\tau}$ by only as much as does the denominator of Eq. (15). Since τ increases from 170 MPa to 415 MPa when the strain is increased from 0.05 to 0.20, Eq. (23)

suggests that ρ_m should decrease by the ratio 170/415. The actual decrease in ρ_m is less than this since both $\sigma/\hat{\tau}$ and f decrease slightly with increasing strain.

The observation that the ratio $\sigma/\hat{\tau}$ remains approximately constant with strain also explains why Eq. (19) was an appropriate choice for the stress dependence of ρ_m. An increase in the mobile dislocation density with stress is consistent with the microstructural model of deformation proposed in Fig. 1. To see this, note that the stress to operate a dislocation source is related to the dislocation line tension T and the spacing between pinned points (or the loop length) L by

$$\sigma = T/bL \ . \tag{24}$$

Thus, higher stresses will yield more dislocations according to the distribution of loop lengths. The suggestion of such a distribution is compatible with the observation that only a small fraction of dislocations are actually mobile at any instant.

6. CONCLUSIONS

In this paper we have examined dislocation mobility through the self-consistent analysis of measurements at high strain rates. We have shown that the increase in rate sensitivity found in copper when the strain rate exceeds $\sim 10^3$ s^{-1} can be interpreted as a transition in rate controlling deformation mechanism. A model of the deformation kinetics has been combined with a measurement of the threshold stress to investigate this transition. The experimental results show close agreement with predictions of the model when the mobile dislocation density is allowed to vary with stress raised to a small power. The mobile dislocation density is found to be relatively independent of strain. These findings are compatible with a simple microstructural model that considers the majority of dislocations to be tied up in tangles separating soft inner regions which are easily traversed by the mobile dislocations.

The influence of dynamic recovery on these conclusions regarding dislocation mobility and on the deformation mechanisms in general remains a question for further investigation.

ACKNOWLEDGEMENT

This work has been performed under the auspices of the U. S. Department of Energy. The authors also wish to extend their gratitude to Duane Wallace who provided helpful suggestions and comments throughout this work and to Charles Frantz for his contribution to the experimental program.

REFERENCES

Aifantis E C and Gerberich W W 1975 Mat. Sci. Engr. 21 107

Clifton R J 1971 Proc. of the Sagamore Conf. on Shock Waves and the Mechanical Properties of Solids ed J J Burke and V Weiss (Syracuse: Syracuse University Press) pp. 73-116

Clifton R J, A Gilat and C-M Li 1983 Proc. of the Sagamore Conf. on Material Behavior Under High Stress and Ultrahigh Loading Rates ed J Mescall and V Weiss (New York: Plenum Press) pp. 1-37

Edington J W 1969 Phil. Mag. 19 1189

Follansbee P S and Frantz C E 1983 J. Engr. Mat. Tech. 105 61

Follansbee P S, Regazzoni G and Kocks U F 1984 To appear in Proc. of 3rd Oxford Conf. on The Mechanical Properties of Materials at High Rates of Strain ed J. Harding (London: Institute of Physics)

Frantz C E, Follansbee P S and Wright W J 1984 To appear in Proc. of 8th Int. Conf. on High Energy Rate Fabrication, Am. Soc. Mech. Engr.

Frost H J and Ashby M F 1971 J. Appl. Phys. 42 5273

Granato A V 1971 Phys. Rev. B 4 2196

Granato A V 1973 Metallurgical Effects at High Strain Rates ed R W Rohde, B M Butcher, J R Holland, and C H Karnes (New York: Plenum Press) pp. 255-273

Hauser F E, Simmons J A and Dorn J E 1961 Conf. on Response of Metals to High Velocity Deformation ed P G Shewmon and V F Zackay (New York: Interscience) pp 93-110

Klahn D, Mukherjee A K and Dorn J E 1970 2nd Int. Conf. on The Strength of Metals and Alloys (Am. Soc. Metals) pp. 951-962

Kocks U F 1975 Constitutive Equations in Plasticity ed A S Argon (MIT Press) pp. 81-115

Kocks U F, Argon A S and Ashby M F 1975 Thermodynamics and Kinetics of Slip, Prog. Mat. Sci. 19 (New York: Pergamon Press)

Kumar A, Hauser F E and Dorn J E 1968 Acta Met. 16 1189

Kumar A and Kumble R G 1969 J. Appl. Phys. 40 3475

Lindholm U S 1971 Measurement of Mechanical Properties V ed R F Bunshah (New York: Interscience) pp. 199-271

Mayer M, Vohringer D and Macherauch E 1980 5th Int. Conf. on Strength of Metals and Alloys (Toronto: Pergamon Press) pp. 807-812

Mecking H and Kocks U F 1981 Acta Met. 29 1865

Orlova A 1981 Scripta Met. 15 119

Seeger A 1955 Phil. Mag. 46 1194

Shioiri J, Satoh K and Nishimura K 1978 Symp. on High Velocity Deformation of Solids ed K Kawata and J Shioiri (New York: Springer-Verlag) pp. 50-66

Tamler H, Heckeloer H J, Kanert O, Alsen W H M and De Hosson J Th M 1981 Nuclear and Electron Resonance Spectroscopies Applied to Materials Science ed E N Kaufmann and G K Shenoy (New York: North Holland) pp. 421-425

Vreeland T Jr. 1968 Dislocation Dynamics ed A R Rosenfield, C T Hahn, A L Bement and R I Jaffee (New York: McGraw-Hill) 283
Weertman J 1973 Metallurgical Effects at High Strain Rates ed R W Rohde, B M Butcher, J R Holland, and C H Karnes (New York: Plenum Press) pp. 319-332

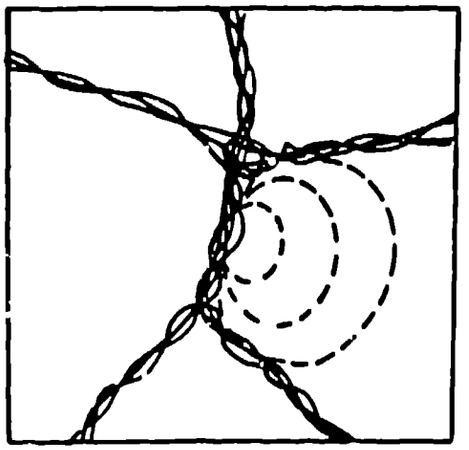

Fig. 1 Schematic of tangled dislocations showing a single loop expanding from the wall, which is one possible mechanism for generating mobile dislocations.

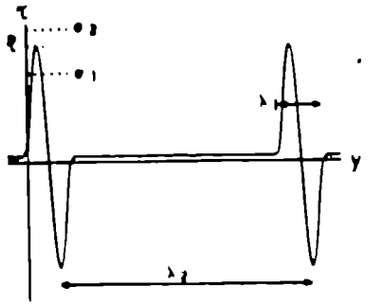

Fig. 2 Typical glide resistance profile.

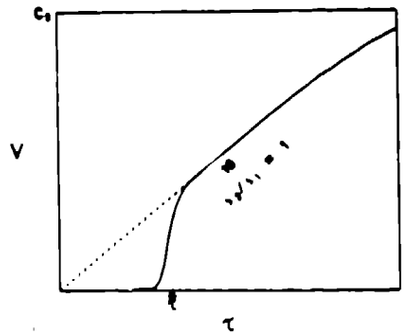

Fig. 3 Stress dependance of the dislocation velocity.

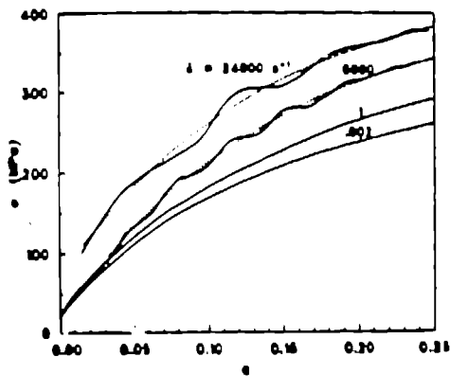

Fig. 4 Static and dynamic stress strain curves for annealed oxygen-free copper

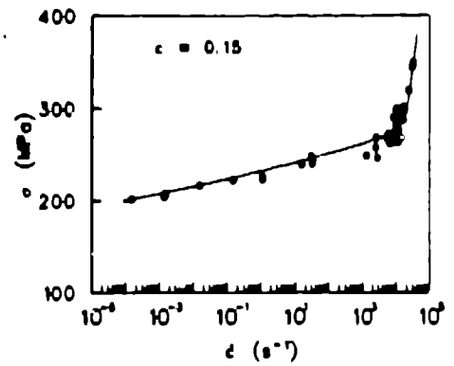

Fig. 5 Strain rate dependence of the flow stress of copper.

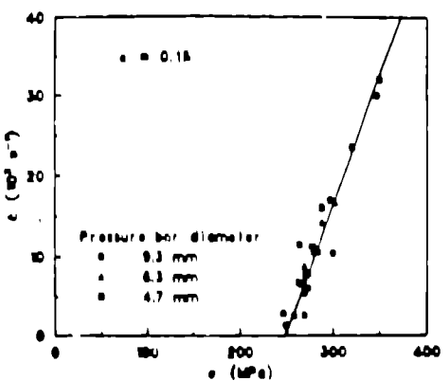

Fig. 6 Strain rate dependence of the flow stress of copper

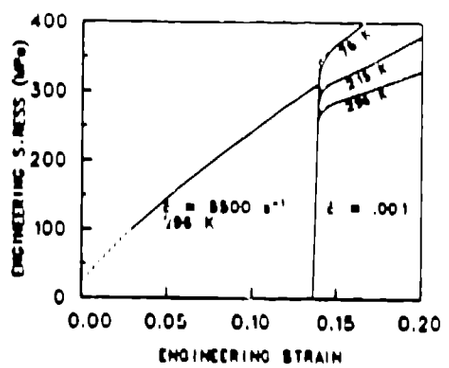

Fig. 7 Measurement of the threshold stress loading history.

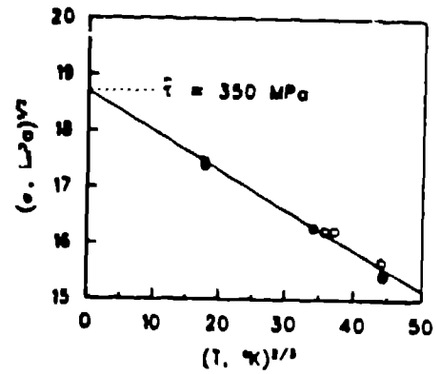

Fig. 8 Measurement of the threshold stress: extrapolation to 0 K.

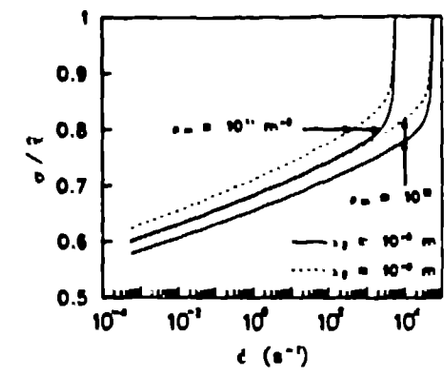

Fig. 9 Predictions of the model as a function of λ_2 and ρ_m.

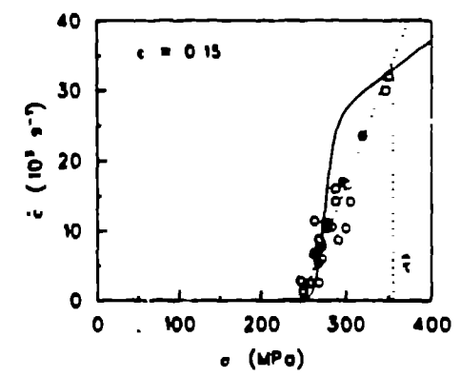

Fig. 10 Comparison of the model with the experimental results.

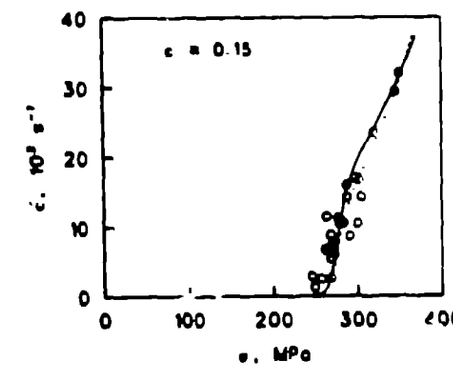

Fig. 11 Comparison of the experimental results with predictions of the model when ρ_m is varied according to Eq. (19).

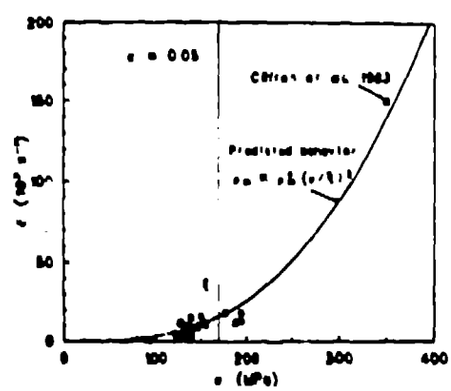

Fig. 12 Comparison of the model with data point from pressure-shear experiment (Clifton et al, 1983).

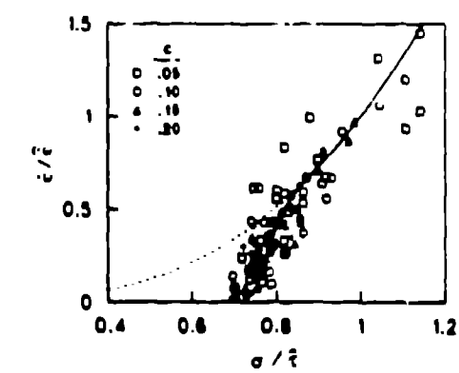

Fig. 13 Experimental results for strains of .05 to .20 and prediction of the model for normalization given in Eq. (20).